Manufacturing Miniature Langmuir probes by Fusing Platinum Bond Wires

Martin Berglund[1]*, Peter Sturesson[1,2], Greger Thornell[1], and Anders Persson[1]

[1]Ångström Space Technology Centre, Dept. of Engineering Sciences, Uppsala University, Uppsala, Sweden
[2]Div. of Military Technology, Dep. of Military Sciences, Swedish Defence University, Stockholm, Sweden

Submitted to Journal of Micromechanics and Microengineering, 2015

Abstract

This paper reports on a novel method for manufacturing microscopic Langmuir probes with spherical tips from platinum bond wires by fusing for plasma characterization in microplasma sources. Here, the resulting endpoints, formed by droplets on the ends of a fused wire, are intended to act as a spherical Langmuir probes. For studying the fusing behavior, bond wires were wedgebonded over a 2 mm wide slit, to emulate the final application, and fused with different voltages and currents. For electrical isolation, a set of wires were coated with a 4 µm thick layer of Parylene before they were fused. After fusing, the gap size, as well as the shape and area of the ends of the remaining stubs were measured. The yield of the process was also investigated, and the fusing event was studied using a high-speed camera for analyzing its dynamics. Four characteristic tip shapes were observed: spherical, folded, serpentine shaped and semi-spherical. The stub length leveled out at ∼400 µm as the fusing power increased. The fusing of the coated wires required a higher power to yield a spherical shape. Finally, a Parylene coated bond wire was integrated into a stripline split-ring resonator (SSRR) microplasma source, and was fused to form two Langmuir probes with spherical endpoints. These probes were used for measuring the I-V characteristics of a plasma generated by the SSRR. In a voltage range between -60 V and 60 V, the fused stubs exhibited the expected behavior of spherical Langmuir probes, and will be considered for further integration.

I. Introduction

Wire bonding has in recent years found many applications outside the traditional use as interconnections in the integrated circuit industry. Standard mounting techniques includes ultrasonic wedge bonding, thermosonic ball-stitch bonding and ball bumping [1]. Gold, aluminum, and copper are the most common wire materials due to their favorable mechanical properties and high electrical conductivity.

Examples of new applications include the reports of Schröder et al. on a method for ball-stitch bonding of a 20:1 aspect ratio through-silicon via using a 20 µm thick gold wire [1]. Kratt et al. have developed a method for manufacturing microscale coils using ball-stitch bonding along a solenoid path [2]. From that study, Badilta et al. developed a double-coil bearing system, using magnetic levitation for elevating a microscale metal platform [3]. In a slightly different approach, Pai et al. have presented ball bumps that are nanoimprinted with silicon stamps [4], and Yabuki and Tea have patented a novel use of stacked ball bump walls as electrical interfaces orthogonal to flat conductor patterns for edge connections [5].

The ability of bond wires to handle high power peaks without failure has also been studied. Nieberlein has calculated and evaluated the heat distribution and voltage levels for failures of 25-µm diameter gold and aluminum wires [6]. Loh has presented numerical models based on current and fusing time data, [7]. His results suggests that heat dissipation in 25 µm thick wires is primarily dominated by convection, followed by conduction and radiation with proportions of 54:10:1. Coxon et al. have refined the modeling of Loh [8], and argue that even though Nieberlein did not account for convection and radiation losses, the temperature profile trends for increasing voltage in [6] should remain the same.

Since fused bond wires may attain a spherical droplet at the end of the stub left after fusing, as shown in [9], they can potentially act as microscale spherical Langmuir probes. In [10, 11, 12], a concept employing a microplasma source with integrated cylindrical Langmuir probes for carbon isotope measurements measuring an optogalvanic signal was reported on. The plasma source was fabricated on printed circuit board, and the Langmuir probes were made from 25 µm thick gold wires, by letting the tails of the bonded wires protrude into the plasma.

This system is going to be integrated into a complete lab-on-a-chip device, including a sub-system for sample preparation as reported in [13]. Therefore, High-Temperature Co-Fired Ceramic (HTCC) is considered as the new substrate material [14]. HTCC devices exhibit several advantages, being heat sustainable and free from carbon that can contaminate the plasma.

*martin.berglund@angstrom.uu.se

Platinum is the most common conductive material in HTCC, having a melting point well above the typical sintering temperatures of 1500 °C. Hence, platinum bond wires can potentially survive the sintering, and be integrated as Langmuir probes in an HTCC plasma source. However, such wires would have to be attached before sintering, and it is next to impossible to bond wires in this phase of the fabrication. Hence, a new technique for attaching the probes is required.

Stretching a wire over the gap and letting it be integrated with the alumina and platinum of the device is one option. This would provide mechanical robustness during manufacturing, and the wire would potentially not curl during sintering. Such an approach would, however, require fusing of the platinum wire into two separate probes after sintering.

This paper presents a study on fusing of 25 µm thick platinum bond wires into microscale spherical Langmuir probes, and a process of integrating them into a stripline split-ring resonator (SSRR) microplasma source. Bond wires were fused using a set of different currents and voltages, and the resulting gap size, area and shape factor of the endpoints formed on the stubs were evaluated. For dynamic studies of the fusing event, high-speed camera footage was captured. A method for isolating the wires using Parylene was also investigated, and Langmuir probes manufactured in this way were integrated into the SSRR, and used to characterize its plasma.

II. Materials and Methods

The bond wires used in this study were 25 µm think 99.99% platinum wires, P14834PM, Semiconductor Packaging Materials, USA. They were bonded onto custom-made FR4 printed circuit boards (PCBs), 16 parallel wires on each, figure 1, using a 4526 wedge wire bonder, Kulicke & Soffa Industries, Singapore. The wires spanned a 2 mm wide slit in the PCB in order to resemble the hole through the plasma source [10]. The lateral distance between the two bonds of the wires was 2.7 mm and the wire length was 2.85 mm. A total of 224 wires were bonded onto 14 PCBs.

The fusing was performed using a power supply, TTI QL355P, Thurlby Thandar Instruments, UK, controlled by a custom-made Matlab script. All fusing was performed at atmospheric pressure and room temperature, except for 16 wires that were fused at reduced pressure (∼5 Torr) in a vacuum chamber, to study the effect of convection.

An oscilloscope, InfiniVision DSO7104A, Agilent, USA, was used to measure the current and voltage during fusing. The voltage, U, over the connection to the array chip was monitored and the voltage over a ballast resistor of 1.6 Ω, in series with the array chip was monitored simultaneously. From the voltage over the ballast resistor and the resistor value the current, I, flowing through the wire, was calculated.

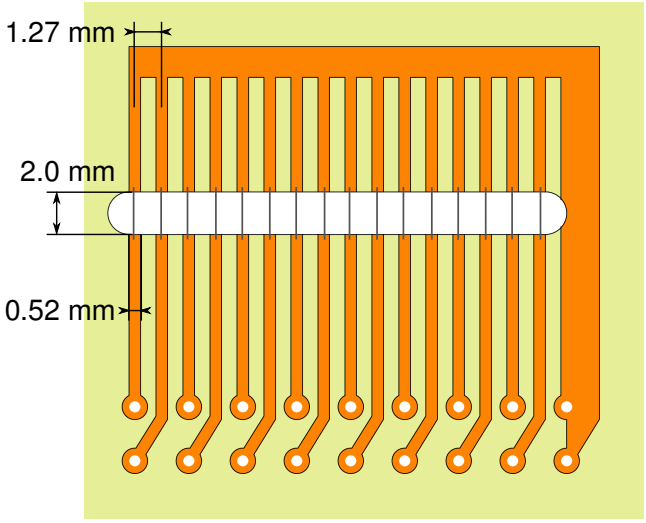

Figure 1: *Layout of a PCB with 16 platinum bond wires.*

The length of the gap between the two stubs formed after fusing was measured from a microscope image of the wires, captured orthogonal to the PCB surface.

The fused wires were inspected by scanning electron microscopy (SEM), Zeiss 1550, Zeiss, Germany, to study the endpoints of the remaining stubs. Each stub was studied separately, and the SEM pictures were analyzed using Matlab to estimate the area and shape of the endpoints, excluding the wire leading up to the droplet. Again, the stubs were investigated orthogonally to the PCB surface. The shape factor of an endpoint was defined as the ratio between the minor and major axes of the smallest ellipse that could enclose the entire shape. Hence, a shape factor of 1 corresponds to a spherical endpoint, although only a projection of the endpoint was investigated, and rotational symmetry was assumed for simplicity. A shape factor of 0.5 corresponds to a shape with one dimension twice as long as the other. Stubs without endpoints, this includes most of the serpentine shaped ones discussed below, were noted faulty, and were disregarded in later analysis.

In a first experiment, a total of 64 wires were fused, with different voltage and current limits of the power supply, and the gap between the stubs, and the shape factor and area of the endpoints formed at their ends were measured. A matrix of four voltage limits (3.0, 8.7, 14.3 and 20 V) and four current limits (0.6, 1.3, 2.1 and 3.0 A) was investigated with four replicates in each point.

Another 96 wires were fused using multiple settings

to provide better statistics.

In order to test whether the slit through the PCB affected where the gap in a bond wire formed, one PCB was bonded with about 4 mm long wires that were placed asymmetrically over the slit. After fusing all these wires with the same voltage and current limits, 10 V and 1.6 A, the length of all stubs was measured with a microscope in the same way as above.

The dynamics of the fusing event was studied using a high-speed camera, MIRO M310, Vision Research, USA, mounted on a microscope, capturing 18000 frames per second. The fusing of a total of 16 wires was captured in this way.

A total of 16 wires were coated with 4 µm of Parylene, by chemical vapor deposition in a LAB TOP 3000, Para Tech, USA. In order to improve adhesion, the wires were dip coated in silane, Silquest A-174NT, Paratech Coating, USA, for 30 minutes and cured in an oven at 80 °C for 30 minutes, prior to deposition. A total of 4 grams of Galxyl C, Galento S.r.l., Italy, was used in the deposition, which was performed at a pressure of 5 mTorr. The coating was activated for 220 min at 650 °C.

Another power supply, TTI QL355TP, Thurlby Thandar Instruments, UK, was used to fuse the Parylene coated wires, which required higher power to form equally gaps as their uncoated counterparts. The new fusing parameters, U and I, were empirically mapped, using the high-speed camera setup described above for feedback. The coated wires required 25 V and 5 A to create equivalent results as wires without Parylene fused around 8.7 V and 1.3 A. The results were evaluated in the same way as above.

Finally, a Parylene coated wire was integrated in a SSRR plasma source, resembling those described in [12], but with a 3 mm wide plasma gap. The wire was stretched between the pads in the same manner as with the test array in figure 1, between the two probepads. The wire was fused with a voltage and current limit of 25 V and 5 A, respectively, to form two spherical Langmuir probes, replacing the cylindrical probes used in previous studies [10, 11, 12]. For a description of the positioning of the plasma probes inside the SSRR see [10]. Also, X-ray images of these probes were captured using an XT V 130 Electronics X-ray system, Nikon, Japan.

The plasma source was installed in a vacuum chamber with air to a pressure of about 2 Torr, and ignited using the setup described in [11]. The probes were used to study the I-V characteristics of the plasma, by applying a constant bias voltage, V_B, to one of the probes using a Model 2400 source meter, Keithley Instruments Inc., USA, while connecting the other probe to ground. The bias voltage was varied between -60 V and 60 V, while recording the current, I_B, through the probes with the source meter, in a way similar to that in [12].

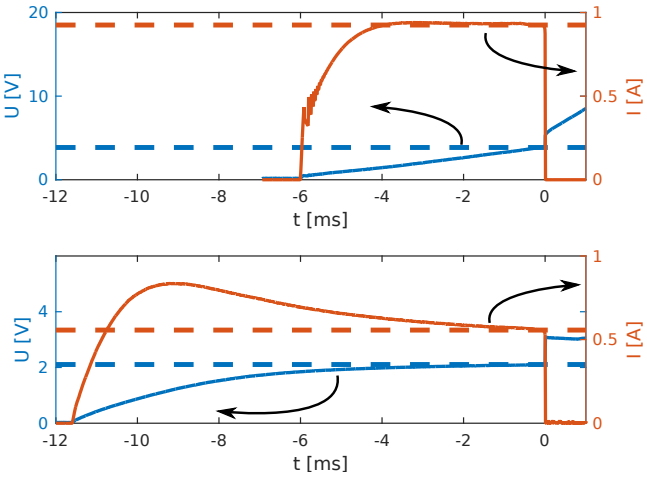

Figure 2: *Voltage, U, and current, I, during the fusing of two platinum bondwires. The fusing occured at 0 s. The two cases where either the current (top) or voltage (bottom) was limited are shown. The current and voltage at the fusing event, used for calculating the fusing power are shown by dashed lines.*

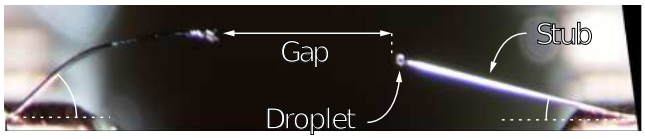

Figure 3: *Platinum wire fused using a power of 0.9 W (top). The length of the gap is 660 µm. The asymmetry of the bonded wire is visible, one side rising more steeply than the other. At the bottom are examples of the four most common shapes of the stub ends including (I) spherical, (II) folded, (III) serpentine, and (IV) semi-spherical.*

Many of the models used to characterize plasma with the help of Langmuir probes set certain restrictions on what what types of plasma that can be characterized and that the probes should not disturb the plasma. Therefore probe measurements in this setup are more useful as a relative tool for comparing different plasma conditions in the same device rather than absolute measurements of the plasma. Therefore, most plasma parameters were not acquired for this particular case, but only the shape of the I-V curve as a confirmation of the function of the new probes, and the plasma potential as it is useful for comparisons. The plasma potential was determined by finding the maximum of the derivative of the current as a function of the bias potential, dV_B/dI_B.

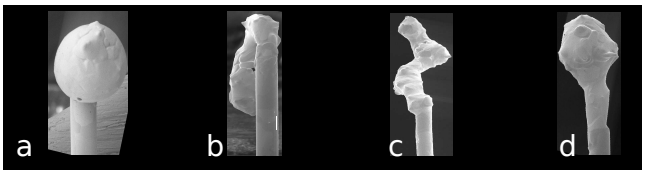

Figure 4: *The four most common shapes of the stub ends including (a) spherical, (b) folded, (c) serpentine, and (d) semi-spherical.*

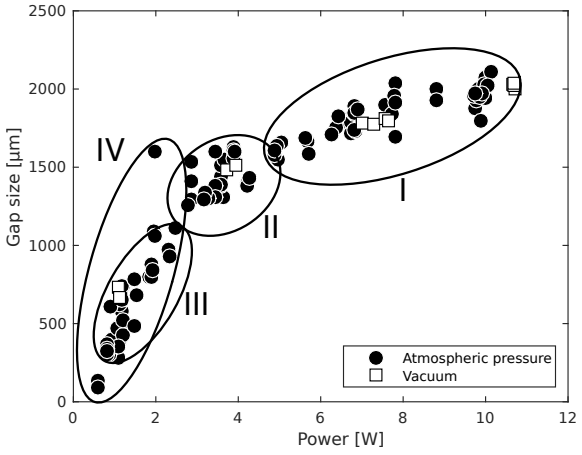

Figure 5: *Gap size versus power at fusing. The experiments performed in vacuum are marked with squares. The regions of the respective endpoint shapes are also highlighted.*

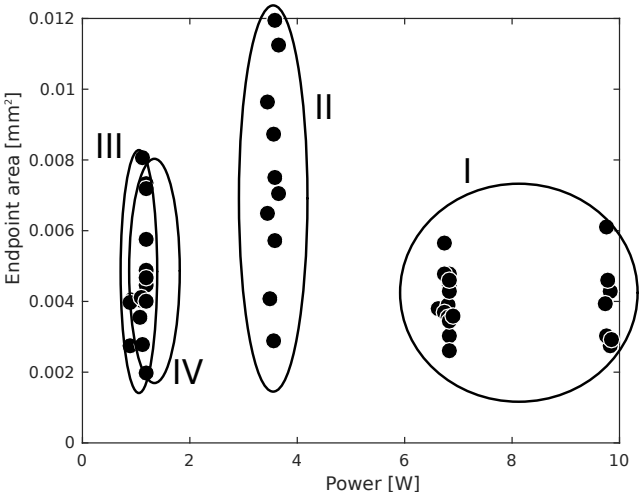

Figure 6: *Area of endpoints after fusing at different power. The regions of the respective endpoint shapes are also highlighted.*

III. Results

As the fusing event is a dynamic process where either the voltage or current is limited while the other parameter follows the resistance change, figure 2, the value of U and I immediately before the fusing, and the corresponding power, are hereafter used to describe the fusing event.

A platinum bond wire fused using a power of 0.9 W, resulting in a 660 µm gap between the remaining stubs, is shown in figure 3. This was in many ways a representative result for all the experiments, although the length of the gap, and the shape of the ends of the stubs varied with the amount of applied power. Figure 4 shows the four most common stub endpoints formed after fusing, varying considerably from almost spherical, which was the aim of this study, to folds and serpentine shapes.

The relationship between the gap size and the applied power is shown in figure 5, with the gap size of wires fused in vacuum shown with squares.

In addition to the gap size, the shape factor and area of the shapes formed at the ends of the fused stubs were investigated, figure 6 and 7. However, the ends of stubs that were missing droplets as endpoints after fusing were not characterized. Figure 8 shows the yield of the endpoint droplet formation.

In the investigation whether the slit through the PCB affected the position of the gap, and, hence, the individual length of the resulting stubs, the angle between the stub and the substrate at the bond point was also taken into account. Figure 3 shows the typical situation, where one of the stubs rose from the substrate at a much higher angle than the other. This difference was not caused by the fusing, but by the initial bond-

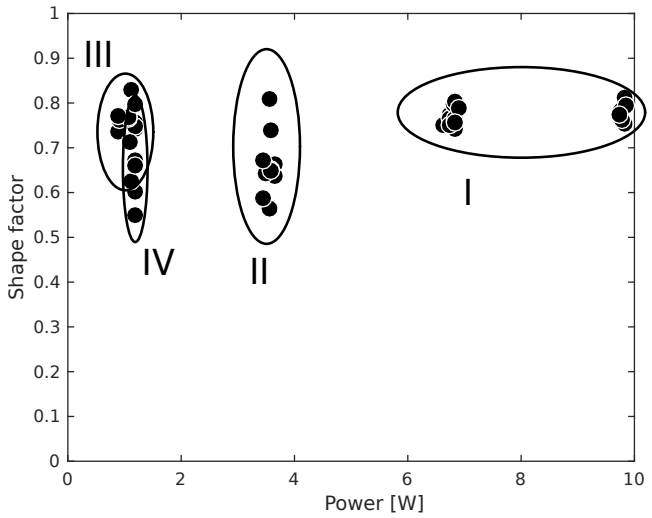

Figure 7: *Shape factor of the droplets sticking to the endpoints after fusing. The regions of the respective endpoint shapes are also highlighted.*

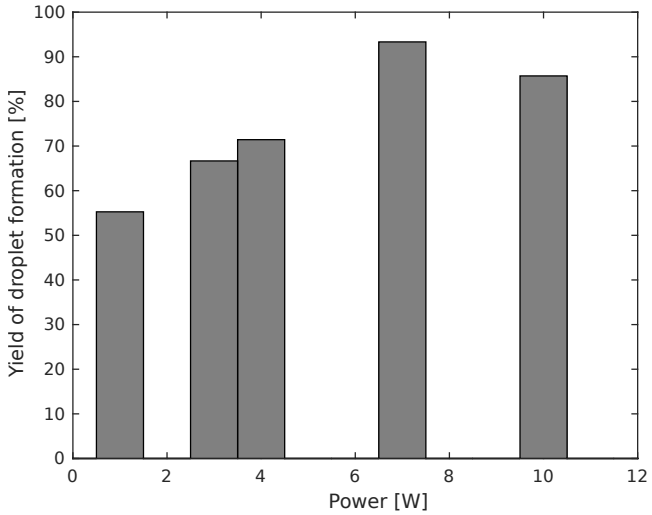

Figure 8: *Yield of droplet formation at wire endpoints versus fusing power.*

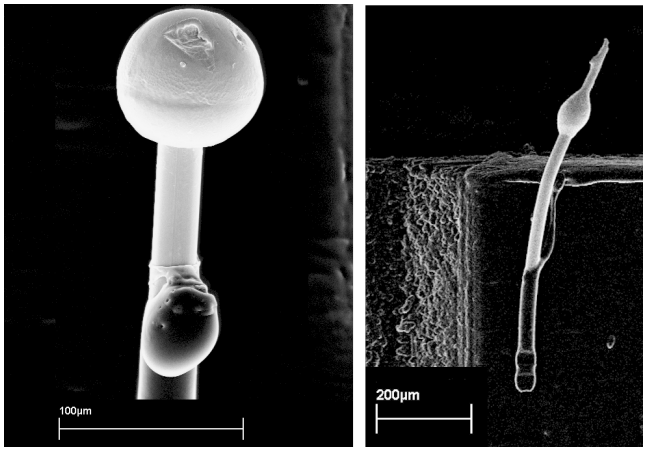

Figure 10: *Stubs of Parylene coated platinum wires, fused with ∼23 W (left), and ∼6.5 W (right). The values for these fusings were not logged but rather extrapolated from other logged events.*

ing of the wire. It was found that the length of the stubs rising at a higher angle was not affected by the distance between the bond point and the slit, where the average length of the stubs was 650 µm±40 µm (1σ). The length of the stubs rising at a low angle received a similar average regardless of the position of the bond, however, for those with bonds longer from the slit than the average stub length, the variations in length increased considerably, as seen from a much larger standard deviation of 198 µm.

The high-speed camera was able to record the fusing event with good resolution, figure 9. Video sequences of four events, representative of different fusing mechanisms, have been submitted as supplementary data.

Fusing wires coated with Parylene required more power compared with uncoated ones, especially in order to form spherical tips. A stub fused with a voltage limit of 25 V and a current limit of 5 A can be seen in figure 10 (left), where the remaining Parylene can be seen further down the stub. The relationship between the area of the endpoints and that of the exposed part of the stub was 4:1, in this case. At lower power, it was found that the core of the wire did not melt as quickly as the surface, making the resulting entpoint look impaled on the stub, figure 10 (right).

The Parylene coated wire that was integrated in the SSRR plasma source formed two stubs with spherical endpoints, figure 11 (inset), although one of them was slightly impaled. When powering the plasma source, the stubs yielded stable and reliable I-V measurements, figure 11.

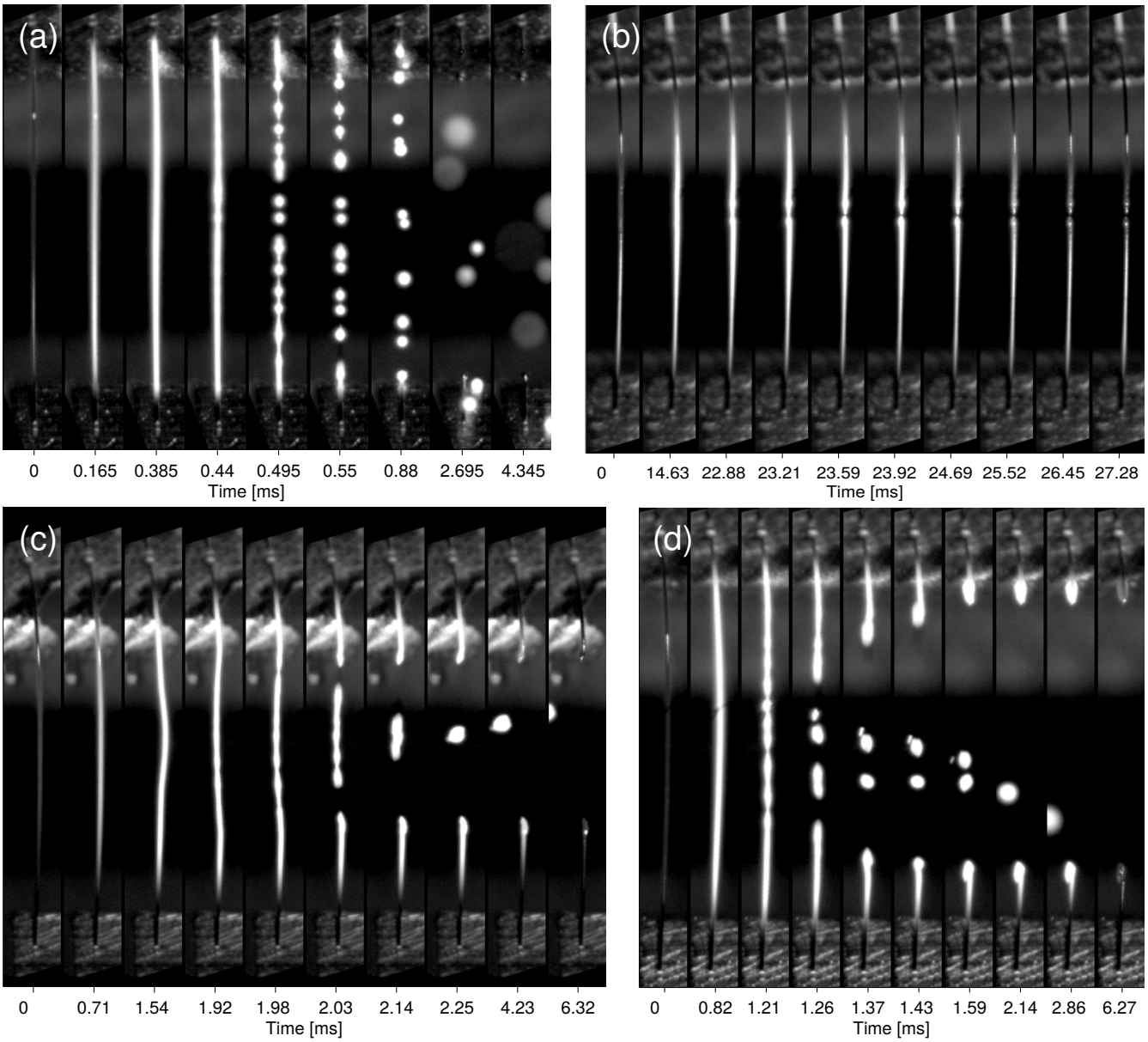

Figure 9: *Frames from high-speed camera footage of the wire fusing. ∼10 W (a), ∼0.6 W (b), ∼2.8 W (c), and ∼5.0 W (d), were used. The time axes are not linear.*

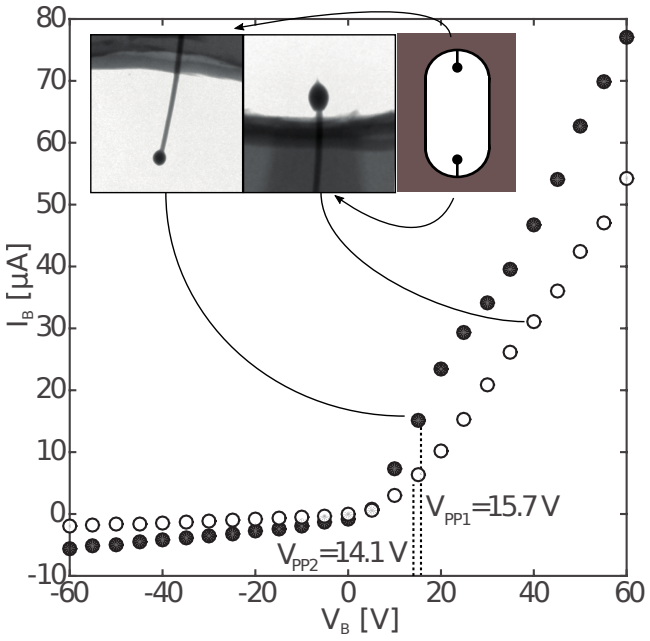

Figure 11: *I-V curves of two Parylene coated probes in a 2 Torr plasma of air. The insets show X-ray images of the probes and their respective placement in the plasma gap.*

IV. Discussion

The rate of change of gap sizes compared with applied power in figure 5 starts to level out as it approaches the maximum gap length of 2700 μm. This is an indication of that much of the heat is conducted from the wire into the substrate. This was further supported by the vacuum measurement which showed that a reduced pressure had no significant effect on the gap size.

Interestingly, it was the fusing at high-power that produced the most spherical and most consistent endpoints, with the best yield, figure 7 and 8. Hence, high power fusing offered both good results and control for fabricating spherical Langmuir probes.

However, far from all wires received spherical endpoints. Instead, four prominent fusing mechanisms were observed in the study, figure 5, each producing a characteristic stub shape, figure 4. Combining the results in figure 5, 6, and 7 with SEM images and high-speed camera footage, four different regions, each defined by one such fusing mechanism, were identified.

Region I corresponds to the previously discussed high-power region, where mostly spherical endpoints were formed on the tips of the stubs, similar to figure 4 (a). Studying the fusing event with the high-speed camera revealed that a large part of the wire melted in a very rapid fashion, figure 9 (a). The melted wire formed several small droplets that were ejected in seemingly random directions. However, the droplets that formed near the stubs were pulled onto their ends, and quickly solidified. Hence, the area of the endpoints in this region was consistently small, figure 6, since most of the material of the melted wire was not added to the stubs.

In region II, roughly corresponded to a power between 2.5 and 4.5 W, large, often elongated endpoint was folded back along the remaining stub after fusing, figure 4 (b). The high-speed camera revealed that more material was lost than in Region III, but the reason for the endpoint to fold instead of curl, as in Region III, is not obvious. However, more kinetic energy was involved in the droplet formation here compared with in Region IV, figure 9 (d). Region II displays the largest but most irregular endpoints of the study, figure 6 and 7.

Region III corresponds to low power where the voltage limited the fusing. Here, predominantly serpentine shaped stub ends were formed, figure 4 (c). With the high-speed camera, it was seen that only a small part of the wire was melted in this region, and that no or negligible material was lost due to the ejection of droplets, figure 9 (b). Instead, when the wire broke, the stub on each side pulled back and the nearly melted material at their ends solidified in the serpentine shape.

Finally, Region IV corresponds to a current limited fusing below 3 W. Here, one of the stubs generally formed a semi-spherical endpoint, whereas the other did not retain any material, figure 4 (d). The high-speed camera revealed that some material was lost in the fusing in this region, where the middle part of the bond wire melted into a large droplet and fell away, after which the two endpoints slowly retracted and solidified, figure 9 (c). The material lost probably corresponds to the part of the wire that formed serpentine shapes in Region III. The cooler event, due to the lower power, was probably the reason for the shape being less spherical than in Region I. Since this kind of stub end was considered faulty, the yield in this region was the lowest, figure 8.

Fusing wires coated with Parylene required significantly more power in order to achieve the spherical endpoints. This might be due to the extra energy needed to evaporate the Parylene. Moreover, the overall trend was that the core of the wires was less prone to melting than the surface. This effect was not observed for the uncoated wires, and made the droplets to be impaled on the stubs, figure 10 (right). The Parylene left on the stubs after fusing consistently reached only a short distance from the bond, and never all the way to the droplet, regardless of the fusing power. However, at sufficiently high power, here 23 W, spherical endpoints on stubs mostly covered by Parylene could be formed,

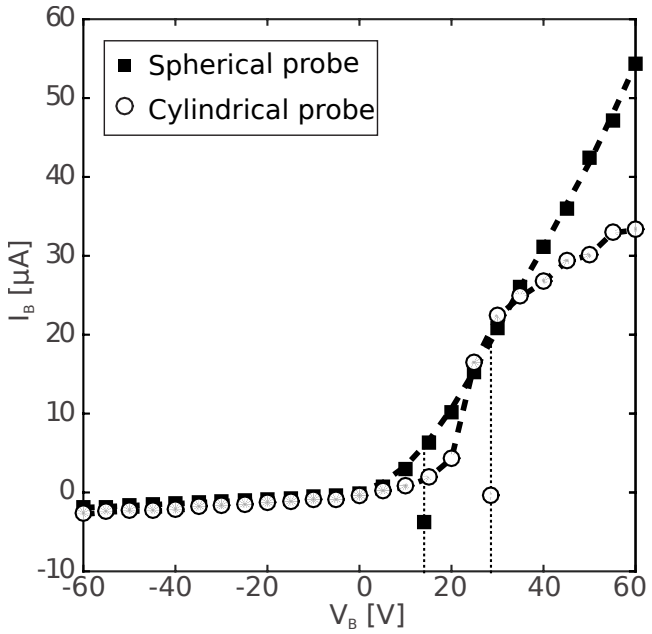

Figure 12: *Comparison of I-V curves measured with a spherical probe with Parylene coated stub (black squares) and an uncoated cylindrical probe (white circles). The plasma potential for each measurement is marked by a dotted line.*

figure 10 (left). The values for these fusings were not logged but rather extrapolated from other events given the voltage and current settings.

Figure 12 shows a comparison between one of these probes and a cylindrical probe from [12] when evaluated as Langmuir probes in the SSRR plasma source. From Langmuir probe theory, it is evident that a properly functioning, spherical Langmuir probe should exhibit a higher saturation current at positive bias above the plasma potential compared with a cylindrical one [15]. This was clearly visible in the I-V curves. Together, these results indicated that the fabrication process described here can be used to create well-functioning Langmuir probes for plasma analysis.

Later, the fusing process will be used together with HTCC manufacturing of SSRR microplasma sources for optogalvanic spectroscopy [14].

V. Conclusions

It was found that the length of the stubs of the fused wire could be controlled by the applied power, but that there was a limit to the gap size, governed by cooling from the substrate, that made the gap size level out at 2 mm, leaving a ∼400 μm long stub at each end, at high power. Endpoints of different shapes and sizes were formed at the ends of the stubs depending on the fusing parameters. Four principal endpoint formations were observed, where one produced spherical endpoints suitable for the Langmuir probes.

Moreover, coating the wires in Parylene before fusing, provided insulation of the probes, but increased the power required to form the spherical endpoints. Probes manufactured in this way, were found to perform well as Langmuir probes.

Acknowledgments

The authors would like to thank the Swedish National Space Board (SNSB) for funding this project. The Knut and Alice Wallenberg foundation is acknowledged for funding additional laboratory facilities. All contributions from Stefan Knaust, Martin Andersson, and Lena Klintberg at the Division of Microsystems Technology, Uppsala University, are also very much appreciated.

References

[1] S. Schröder, A. C. Fischer, G. Stemme, and F. Niklaus. Very high aspect ratio through silicon vias (tsvs) using wire bonding. In *Solid-State Sensors, Actuators and Microsystems (TRANSDUCERS & EUROSENSORS XXVII), 2013 Transducers & Eurosensors XXVII: The 17th International Conference on*, pages 167–170. IEEE, 2013.

[2] K. Kratt, V. Badilita, T. Burger, J. G. Korvink, and U. Wallrabe. A fully mems-compatible process for 3d high aspect ratio micro coils obtained with an automatic wire bonder. *Journal of Micromechanics and Microengineering*, 20(1):015021, 2010.

[3] V. Badilita, S. Rzesnik, K. Kratt, and U. Wallrabe. Characterization of the 2 nd generation magnetic microbearing with integrated stabilization for frictionless devices. In *Solid-State Sensors, Actuators and Microsystems Conference (TRANSDUCERS), 2011 16th International*, pages 1456–1459. IEEE, 2011.

[4] R. Pai, M. Crain, and K. Walsh. Maskless shaping of gold stud bumps as high aspect ratio microstructures. *Microelectronic Engineering*, 88(1):135–139, 2011.

[5] R. Yabuki and N. Tea. Stacked contact bump, May 27 2008. US Patent 7,378,734.

[6] V. A. Nieberlein. The heating and failure of microelectronic wires from an electric pulse. Technical report, DTIC Document, 1982.

[7] E. Loh. Physical analysis of data on fused-open bond wires. *Components, Hybrids, and Manufacturing Technology, IEEE Transactions on*, 6(2):209–217, 1983.

[8] M. Coxon, C. Kershner, and D. McEligot. Transient current capacities of bond wires in hybrid microcircuits. *Components, Hybrids, and Manufacturing Technology, IEEE Transactions on*, 9(3):279–285, 1986.

[9] A. Mertol. Estimation of aluminum and gold bond wire fusing current and fusing time. *Components, Packaging, and Manufacturing Technology, Part B: Advanced Packaging, IEEE Transactions on*, 18(1):210–214, 1995.

[10] M. Berglund, G. Thornell, and A. Persson. Microplasma source for optogalvanic spectroscopy of nanogram samples. *Journal of Applied Physics*, 114(3):–, 2013.

[11] A. Persson, M. Berglund, G. Thornell, G. Possnert, and M. Salehpour. Stripline split-ring resonator with integrated optogalvanic sample cell. *Laser Physics Letters*, 11(4):045701, 2014.

[12] A. Persson, M. Berglund, and M. Salehpour. Improved optogalvanic detection with voltage biased langmuir probes. *Journal of Applied Physics*, 116(24):–, 2014.

[13] Z. Khaji, P. Sturesson, K. Hjort, L. Klintberg, and G. Thornell. Investigation of the storage and release of oxygen in a cu-pt element of a high-temperature microcombustor. *Journal of Physics: Conference Series*, 557(1):012078, 2014.

[14] M. Berglund, A. Persson, and G. Thornell. Evaluation of dielectric properties of htcc alumina for realization of plasma sources. *Journal of Electronic Materials*, 2015.

[15] W. R. Hoegy and L. H. Brace. Use of langmuir probes in non-maxwellian space plasmas. *Review of Scientific Instruments*, 70(7):3015–3024, 1999.